The Astrophysical Journal, 637:494–505, 2006 January 20

FIRST RESULTS FROM THE CHARA ARRAY. III. OBLATENESS, ROTATIONAL VELOCITY, AND GRAVITY DARKENING OF ALDERAMIN

G. T. van Belle[1] and D. R. Ciardi
Michelson Science Center, California Institute of Technology, 770 South Wilson Avenue, MS 100-22, Pasadena, CA 91125; gerardi@ipac.caltech.edu, ciardi@ipac.caltech.edu

T. ten Brummelaar and H. A. McAlister
Center for High Angular Resolution Astronomy, Department of Physics and Astronomy, Georgia State University, P.O. Box 3969, Atlanta, GA 30302-3969; theo@chara-array.org, hal@chara.gsu.edu

S. T. Ridgway
Kitt Peak National Observatory, National Optical Astronomy Observatories, P.O. Box 26732, Tucson, AZ 85726-6732; ridgway@noao.edu

D. H. Berger,[2] P. J. Goldfinger, J. Sturmann, L. Sturmann, and N. Turner
Center for High Angular Resolution Astronomy, Department of Physics and Astronomy, Georgia State University, P.O. Box 3969, Atlanta, GA 30302-3969; berger@chara-array.org, pj@chara-array.org, judit@chara-array.org, sturmann@chara-array.org, nils@chara-array.org

A. F. Boden and R. R. Thompson
Michelson Science Center, California Institute of Technology, 770 South Wilson Avenue, MS 100-22, Pasadena, CA 91125; bode@ipac.caltech.edu, thompson@ipac.caltech.edu

and

J. Coyne
Cavendish Laboratory, University of Cambridge, Madingley Road, Cambridge CB3 0HE, UK; j.coyne@mrao.cam.ac.uk
Received 2005 May 6; accepted 2005 September 22

ABSTRACT

We present observations of the A7 IV–V star Alderamin (α Cep, HR 8162, HD 203280) from the Georgia State University CHARA Array. These infrared interferometric angular size measurements indicate a noncircular projected disk brightness distribution for this known rapid rotator. The interferometric observations are modeled as arising from an elongated rigid atmosphere, with apparent polar and equatorial radii of $r_p = 0.6753^{+0.0119}_{-0.0135}$ and $r_e = 0.8767^{+0.0293}_{-0.0183}$ mas, respectively, for a difference of 201 $\pm$ 32 μas, and with an axial ratio of $r_e/r_p = 1.298 \pm 0.051$. Using the *Hipparcos* distance of 14.96 $\pm$ 0.11 pc, these angular measures translate to 2.18 $\pm$ 0.05 and 2.82 $\pm$ 0.10 $R_\odot$. The inclination of Alderamin to the line of sight indicated by this modeling is effectively edge-on ($i = 88.2^{+1.8}_{-13.3}$ deg). The star has a true rotational velocity of 283 $\pm$ 10 km s^{-1} ($\sim$83% of breakup velocity) and a polar temperature of roughly 8400 K. Significantly, a necessary aspect of this modeling is a determination of the gravity-darkening coefficient, which at a value of $\beta = 0.084^{+0.026}_{-0.049}$ is consistent with a convective photosphere, as expected for an A7 IV–V star. Our detailed characterization of this object allows us to investigate various scenarios for the angular momentum history of Alderamin and the appropriateness of certain stellar evolution models.

Subject headings: infrared: stars — stars: fundamental parameters — stars: individual (Alderamin) — techniques: interferometric

Online material: color figures

1. INTRODUCTION

The Georgia State University Center for High Angular Resolution Astronomy (CHARA) Array is a six-element optical/infrared interferometer located on Mt. Wilson in southern California. The CHARA Array has six 1 m telescopes operational and has recently completed its first full year of science observations, including observations of stellar diameters, young stellar objects, and rapidly rotating stars. A companion paper (ten Brummelaar et al. 2005) describes the full compliment of technical details of the instrument, and McAlister et al. (2005) details the first science results from the instrument, on the rapid rotator Regulus. CHARA's operational status of having the longest *H*- and *K*-band baselines in the world make it uniquely well suited for observations of main-sequence star absolute diameters.

The star Alderamin (α Cep, HR 8162, HD 203280)[3] is a well-studied object, being one of the 20 brightest A-type stars in the sky and one of the nearer stars to the Sun (Perryman et al. 1997; Cox 2000). Originally classified as an A2n (Douglas 1926), it is now accepted to be an A7 IV–V main-sequence star (Johnson & Morgan 1953) and has been known to be a rapid rotator for over 50 years (Slettebak 1955). The measurements of the star's apparent rotational velocity ($v \sin i$) range from 180 to 200 km s^{-1} (Gray 1980; Abt & Morrell 1995) up to 245–265 km s^{-1} (Bernacca & Perinotto 1970; Abt & Moyd 1973), depending on the spectral lines used in the investigation. These values of $v \sin i$ are a substantial fraction of an A7 V star's critical velocity of no more than 415 km s^{-1} (a velocity that decreases as the object evolves and increases in size; Slettebak 1966), where centripetal acceleration at the stellar equator equals gravitational acceleration.

[1] For reprints, please contact gerard@ipac.caltech.edu.
[2] Michelson Fellow.
[3] VizieR Online Data Catalog, 5050 (D. Hoffleit & W. H. Warren, 1995).

Recent advances in interferometric observations have allowed for direct observation of rotationally oblate main-sequence stellar surfaces, including the first such observation by van Belle et al. (2001) of the A7 IV–V rapid rotator Altair, confirmation of that object's latitude-dependent temperature structure (Ohishi et al. 2004; Peterson et al. 2006), and the CHARA Array observations of Regulus (McAlister et al. 2005). Similar observations of the related Be star phenomenon have also been achieved by interferometers (Quirrenbach et al. 1994; Domiciano de Souza et al. 2003).

The effects of stellar rotation have been measured spectroscopically for almost a century, beginning with Schlesinger (1909, 1911). Models of rotating stars have explored the impact of rotation on both stellar effective temperature (Slettebak 1949) and stellar shape (Collins 1963, 1965; Collins & Harrington 1966). Recently, models have begun to incorporate the effects of differential rotation as a function of stellar latitude (Zahn 1992). Rotation impacts important observable parameters such as photometry (Collins & Smith 1985) and surface brightness distributions, as originally shown by von Zeipel (1924a, 1924b). Rotation has nontrivial implications on stellar evolution, as explored in the various papers by, among others, Claret and Maeder (cf. Martin & Claret 1996; Claret 2000; Maeder 1997, 2000).

Here we report the determination of the overall diameter and projected shape of Alderamin on the sky from near-infrared, long-baseline interferometric measurements taken with the CHARA Array. *Direct observation* of the stellar disk can provide unique insight into basic stellar parameters. The measured angular size in conjunction with the bolometric flux and distance yields constraints on parameters such as latitude-dependent local effective temperature[4] and linear radii, both of which remain quantities poorly established empirically for virtually all stars. Upon fitting a family of rotating models for the projected stellar photosphere on the sky, we further demonstrate that a unique value for $v \sin i$ may be derived from the interferometric data.

The CHARA Array observations that produced these results are discussed in § 2, detailing source selection and observation. In § 3, we detail supporting spectral energy distribution (SED) fits which constrain stellar parameters appropriate for this analysis. The circular symmetry of our check star is then established in § 4, which also allows us to characterize the uncertainties inherent in the visibility data. In § 5, Alderamin's departure from a circular on-sky brightness distribution is established, and in § 6 we demonstrate that inclination, true rotational velocity, and other astrophysical parameters may be derived from Alderamin's oblateness by fitting the data with the appropriate family of Roche models. Finally, in § 7, we examine the astrophysical implications of the best-fit model, such as the possible angular momentum history of the object.

2. OBSERVATIONS

The interferometric observable used for these measurements is the fringe contrast or visibility (squared) of an observed brightness distribution on the sky. Normalized in the interval $[0 : 1]$, a uniform disk (UD) single star exhibits monochromatic visibility modulus in a UD model given by

$$V^2 = \left[\frac{2J_1(\theta_{\rm UD}\pi B\lambda^{-1})}{\theta_{\rm UD}\pi B\lambda^{-1}}\right]^2, \quad (1)$$

[4] We note that a star's "effective temperature" is a globally defined quantity in terms of the stellar luminosity, $L = 4\pi\sigma R^2 T_{\rm eff}^4$. For denoting the temperature associated with specific surface elements of the stellar surface, we follow the convention of Collins (1963, 1965) and use the term "local effective temperature."

TABLE 1
CHARA Baselines Utilized for Observing Alderamin and Associated Sources

Baseline	Projected Baselines (m)	Projected Sky Angles[a] (deg)	Dates
W1-E1.....	279–312	70–120	2004 Jun 15–21
S1-E1.....	250–304	0–75	2004 Jun 26–29

[a] P.A. is east of north.

where J_1 is the first-order Bessel function, B is the projected baseline vector magnitude at the star position, $\theta_{\rm UD}$ is the apparent UD angular diameter of the star, and λ is the wavelength of the interferometric observation.

Alderamin was observed in the K_s band (0.30 μm wide centered at 2.15 μm) contemporaneously with a primary calibration star, HD 197373, and a check star, HD 211833, by the CHARA Array on eight nights between 2004 June 17 and June 29. Observations of Alderamin were always bracketed within ~20 minutes with the calibration source, and every other Alderamin calibration set included an observation of HD 211833. On the nights of June 17, 19, 20, and 21, Alderamin was observed with the W1 and E1 pair of CHARA telescopes; on June 26–29, the S1 and E1 pair was utilized; details are given in Table 1. Data collection on the nights between June 22 and 25 was attempted with the W1 and S1 pairing, but due to weather and instrumental difficulties, these data were of insufficient quality for this study and were discarded. Other nights between June 17 and 29 were lost to weather and instrument problems. Our check star, HD 211833, was selected on the basis of an expected angular size similar to Alderamin, in addition to an expectation of circular symmetry in its sky projection, based on its low $v \sin i$. Alderamin and HD 211833, along with an "unresolved" calibration object, HD 197373, were observed multiple times during each of these nights, and each observation set, or scan, was approximately 180 s long, consisting of 200 scans. Following commonly accepted and expected optical interferometry practice (van Belle & van Belle 2005), we attempted to achieve absolute instrument calibration through the use of a calibration object that matched the instrument's resolution limit and limiting accuracy, as demonstrated by night-to-night repeatability.

For a 0.41 mas calibration source such as HD 197373, the CHARA Array's longest baseline at 330 m should give a raw V^2 of 0.80 before instrumental and atmospheric degradation. For each scan we computed a mean V^2 value from the scan data, and the error in the V^2 estimate from the rms internal scatter (ten Brummelaar et al. 2005). Alderamin was always observed in combination with its calibration or check sources within 5° and 6.°8 on the sky, respectively. The calibration source HD 197373 is expected to be nearly unresolved by the interferometer with a predicted angular size of 0.41 ± 0.04 mas (computed in § 3); expected angular size and error were based on fitting template SEDs of the proper spectral type from Pickles (1998) to available broadband photometry, particularly in the near-infrared.[5] Since many stars deviate significantly from blackbody behavior and/or have significant reddening (Blackwell & Lynas-Gray 1998), we expect this approach to provide significantly better estimates of calibrator angular size than a simple blackbody fit. These objects were also selected to be slow apparent rotators, with $v \sin i < 30$ km s^{-1} (Uesugi & Fukuda 1982; Henry et al.

[5] VizieR Online Data Catalog, 2209 (D. Y. Gezari et al., 1996) and VizieR Online Data Catalog, 2246 (R. M. Cutri et al., 2003).

TABLE 2
STARS OBSERVED WITH CHARA

Source	θ_{SED}[a] (mas)	Distance from Alderamin (deg)	Spectral Type	$v \sin i$ (km s^{-1})	Notes
Alderamin.....	1.36 ± 0.04		A7 IV–V	~200	Primary target
HD 197373	0.412 ± 0.019	5.0	F6 IV	30	Primary calibrator
HD 211833.....	1.34 ± 0.06	6.8	K3 III	2	Resolved check star

[a] Estimated angular size from SED fitting as described in § 3.

2000). Table 2 summarizes the general parameters for the objects observed in this investigation.

Interferometer V^2 value's were obtained by recording a photometric signal of the two telescope combined beam as the interferometer delay lines were slewed through the white-light fringe position on the sky at a preset group velocity. This signal was normalized with a low pass filter, and a power spectrum was computed. Using calibration scans of the individual beams and the closed shutter, the noise bias was removed from the power spectrum, and the integration of the power results in an estimate of instrumental V^2. An additional correction for atmospheric turbulence visibility bias is also used to adjust this V^2; these steps are all described in mathematical detail in ten Brummelaar et al. (2005). Formal errors for each measure of V^2 were established from the measurement statistics associated with these photometric signals.

The atmospheric calibration of Alderamin V^2 data on the sky is performed by estimating the interferometer system visibility (V^2_{sys}) using the calibration source with model angular diameters and then normalizing the raw Alderamin visibility by V^2_{sys} to estimate the V^2 measured by an ideal interferometer at that epoch (Mozurkewich et al. 1991; Boden et al. 1998). Multiple observations of the calibration source were averaged together in a time-weighted sense, with the error variance being doubled for a 1 hr time separation. Uncertainties in the system visibility and the calibrated target visibility were propagated through the data stream using standard error propagation calculations. This atmospheric calibration process was accomplished through the use of the publicly available wbCalib program.[6]

The formal errors reported by the instrument measurement process are always smaller than those created by the atmospheric calibration process, which is discussed further in § 4. More detail on the CHARA Array's target and calibrator selection, data reduction, and technical aspects is available in the literature (see McAlister et al. 2005; ten Brummelaar et al. 2005). Calibrating our Alderamin data set with respect to the calibration object listed in Table 2 results in a total of 41 calibrated scans on Alderamin over the eight observing nights in 2004, and 22 calibrated scans on HD 211833 over the same nights. Our calibrated V^2 measurements for Alderamin and HD 211833 are summarized in Tables 3 and 4, respectively.

3. SPECTRAL ENERGY DISTRIBUTION FITTING

For each of the three stars observed in this investigation, a SED fit was performed. This fit was accomplished using photometry available in the literature as the input values, with template spectra appropriate for the spectral types indicated for the stars in question. The template spectra from Pickles (1998) were adjusted by the fitting routine to account for the overall flux level, wavelength-dependent reddening, and expected angular size. Reddening corrections were based on the empirical reddening determination described by Mathis (1990), which differs little from van de Hulst's theoretical reddening curve number 15 (Johnson 1968; Dyck et al. 1996). Both narrowband and wideband photometry in the 0.3–3 μm were used as available, including Johnson *UBV*[7] (Eggen 1963, 1972; Moreno 1971), Stromgren *ubvyβ* (Crawford et al. 1966; Piirola 1976), 2Mass *JHK$_s$*,[8] Vilnius *UPXYZS* (Zdanavicius et al. 1969; Zdanavicius et al. 1972), and *WBVR* (Kornilov et al. 1991); flux calibrations were based on the values given in Cox (2000). The results of the fitting are given in Table 5, and an example SED fitting plot is given in Figure 1.

The utility of this fitting was twofold. First, for our calibration source, HD 197373, an a priori estimate of its size is necessary to account for residual resolution that may be afforded by the interferometer's extraordinarily long baselines. With an expected limb-darkened size of $\theta_{est} = 0.412 \pm 0.019$ from the SED fit, HD 197373 has a predicted V^2 of 79.8% ± 1.7% for a 330 m baseline used at 2.2 μm; we consider this size effectively identical to its UD size, since for an F-type size, the difference between the two is at the 1% level (Davis et al. 2000; Claret & Hauschildt 2003), which is far less than our size estimate error. Ideally, a calibration source would be sufficiently pointlike that its V^2 would be indistinguishable from unity, but unfortunately the current system sensitivity does not afford that option. The uncertainty in the calibrator visibility represents one of the fundamental limitations of the system visibility accuracy. However, our current selection of calibrator is sufficiently small in diameter that there are no concerns about a varying system calibration due to unaccounted-for calibrator surface morphology.

Second, SED fitting provides us with an accurate characterization of the stellar bolometric flux. In the case of our check star, HD 211833, the combination of that flux and an actual measure of the star's angular size allows for a direct calculation of the star's effective temperature in § 4 (rather than the model value used to numerically fit the template). Such an analysis is also applied in § 5.2 to our primary target, Alderamin, but as discussed in that section, a single effective temperature is insufficient to characterize the star at the level of detail at which we will be examining it.

We note that the indicated spectral type and luminosity class for HD 211833 is that of K3 III (Bidelman 1957; Schmitt 1971), or of a K1 III (Wright et al. 2003), but that in Table 6, we indicate its best-fit spectral template was for a K0–1 II star with a SED fitting χ^2 per degree of freedom (dof) of 0.69, indicating perhaps some uncertainty in not just its spectral type but true luminosity class. Fits of the "normal" K1 through K3 giant models from Pickles (1998) indicate χ^2/dof values of 7.01,

[6] Detailed documentation and downloads available online at http://msc.caltech.edu.

[7] VizieR Online Data Catalog, 2182 (T. Oja, 1996).

[8] VizieR Online Data Catalog, 2246 (R. M. Cutri et al., 2003).

TABLE 3
THE OBSERVED DATA FOR ALDERAMIN

MJD	Projected Baseline (m)	Position Angle (deg)[a]	Hour Angle (hr)	Normalized V^{2}[b]	Uniform Disk Angular Size (mas)
53173.363.....	279.16	112.8	−2.73	0.0323 ± 0.0068	1.579 ± 0.033
53173.385.....	287.16	105.3	−2.21	0.0145 ± 0.0034	1.632 ± 0.027
53173.415.....	296.88	95.3	−1.48	0.0062 ± 0.0015	1.651 ± 0.018
53173.448.....	305.03	84.9	−0.70	0.0120 ± 0.0023	1.554 ± 0.018
53173.472.....	309.28	77.4	−0.13	0.0045 ± 0.0009	1.605 ± 0.013
53175.376.....	285.87	106.5	−2.29	0.0167 ± 0.0038	1.624 ± 0.027
53175.421.....	299.99	91.7	−1.21	0.0088 ± 0.0020	1.607 ± 0.020
53175.434.....	303.27	87.5	−0.89	0.0073 ± 0.0017	1.604 ± 0.019
53175.473.....	310.25	75.1	0.05	0.0059 ± 0.0013	1.583 ± 0.016
53176.383.....	289.27	103.2	−2.06	0.0124 ± 0.0034	1.635 ± 0.029
53176.398.....	294.11	98.3	−1.70	0.0108 ± 0.0030	1.622 ± 0.027
53176.423.....	301.20	90.2	−1.10	0.0082 ± 0.0023	1.606 ± 0.024
53176.437.....	304.40	85.8	−0.77	0.0051 ± 0.0014	1.623 ± 0.020
53176.462.....	309.13	77.7	−0.15	0.0045 ± 0.0012	1.606 ± 0.018
53176.490.....	312.22	69.0	0.51	0.0029 ± 0.0008	1.613 ± 0.014
53177.437.....	305.05	84.9	−0.70	0.0049 ± 0.0067	1.621 ± 0.138
53177.456.....	308.58	78.8	−0.24	0.0064 ± 0.0057	1.586 ± 0.099
53182.348.....	269.01	50.4	−2.51	0.0425 ± 0.0168	1.594 ± 0.077
53182.446.....	298.31	26.4	−0.16	0.0354 ± 0.0146	1.464 ± 0.068
53182.466.....	301.61	21.3	0.33	0.0690 ± 0.0269	1.341 ± 0.082
53182.482.....	303.69	17.2	0.72	0.0495 ± 0.0195	1.388 ± 0.072
53183.306.....	249.91	60.1	−3.45	0.1114 ± 0.0247	1.502 ± 0.064
53183.322.....	258.10	56.2	−3.07	0.0976 ± 0.0216	1.488 ± 0.058
53183.352.....	271.72	48.8	−2.35	0.0722 ± 0.0150	1.479 ± 0.046
53183.368.....	277.82	45.0	−1.97	0.0607 ± 0.0128	1.481 ± 0.042
53184.327.....	261.74	54.3	−2.89	0.0993 ± 0.0173	1.463 ± 0.045
53184.341.....	268.24	50.8	−2.55	0.0806 ± 0.0141	1.475 ± 0.040
53184.358.....	275.42	46.5	−2.13	0.0660 ± 0.0121	1.478 ± 0.038
53184.381.....	283.38	41.1	−1.59	0.0761 ± 0.0129	1.408 ± 0.036
53184.397.....	288.19	37.2	−1.21	0.0707 ± 0.0127	1.399 ± 0.037
53184.421.....	294.30	31.3	−0.63	0.0608 ± 0.0136	1.398 ± 0.043
53184.433.....	297.02	28.1	−0.32	0.0664 ± 0.0134	1.369 ± 0.039
53184.458.....	301.24	22.0	0.27	0.0715 ± 0.0133	1.337 ± 0.037
53185.375.....	282.19	41.9	−1.67	0.0874 ± 0.0231	1.385 ± 0.062
53185.388.....	286.43	38.7	−1.35	0.0467 ± 0.0142	1.482 ± 0.056
53185.410.....	292.33	33.3	−0.83	0.0725 ± 0.0211	1.374 ± 0.062
53185.419.....	294.64	30.9	−0.59	0.0702 ± 0.0213	1.370 ± 0.063
53185.437.....	298.14	26.6	−0.18	0.0770 ± 0.0235	1.336 ± 0.065
53185.448.....	300.09	23.8	0.09	0.0550 ± 0.0159	1.388 ± 0.053
53185.469.....	303.05	18.6	0.59	0.0398 ± 0.0121	1.425 ± 0.049
53185.481.....	304.40	15.5	0.88	0.0505 ± 0.0151	1.382 ± 0.053

[a] P.A. is east of north.
[b] Errors have been normalized as discussed in § 4.

6.18, and 9.31, respectively; the metal-weak and metal-poor templates show no obvious improvement over these values. However, as is examined in the next section, luminosity class uncertainty does not impact our analysis, in that HD 211833 appears spherical regardless of luminosity class.

4. HD 211833: A "ROUND" CHECK STAR

Before we examine our Alderamin data in detail, we examine the visibility data for our check star, HD 211833. HD 211833 is located in close proximity on the sky to the calibrator and primary target ($\Delta\theta < 7^{\circ}$), and the data collected on all three objects was done in a contemporaneous fashion ($\Delta t < 1^{h}$), with little change expected in the point response of the instrument from scan to scan. One of HD 211833's primary attributes that led to its selection as our check star was a known, low rate of apparent rotation, with $v \sin i = 2\ \mathrm{km\ s^{-1}}$ (de Medeiros & Mayor 1999). From that low $v \sin i$ we inferred that the object would have a circular appearance on the sky, due to either an intrinsic low rotation rate, or a pole-on viewing aspect (see the Appendix). This circular symmetry is independent of uncertainty in the star's luminosity class.

Once normalized values for V^2 have been obtained as described in § 2, the simplest interpretation is to fit a UD angular size to the individual V^2 data points following equation (1). For our check star HD 211833, a single UD fit to the 22 V^2 data points results in an indicated angular size of $\theta_{\mathrm{UD}} = 1.250 \pm 0.009$ mas, with a χ^2/dof fitting value of 13.90. Examination of the HD 211833 UD data as an ellipsoidal sky projection (as detailed in § 5.1 for Alderamin) results in fit values of $2a = 1.252 \pm 0.030$ mas, $2b = 1.172 \pm 0.066$ mas, and $\alpha_0 = 7\overset{\circ}{.}8 \pm 6\overset{\circ}{.}9$, but a reduced χ^2 of $\chi^2/\mathrm{dof} = 13.68$, which represents no significant improvement in fit, and more importantly, a negligible detection of asymmetry.

TABLE 4
THE OBSERVED DATA FOR HD 211833

MJD	Projected Baseline (m)	Position Angle (deg)[a]	Hour Angle (hr)	Normalized V^{2}[b]	Uniform Disk Angular Size (mas)
53173.400.....	277.40	114.8	−2.85	0.1831 ± 0.0422	1.219 ± 0.074
53173.424.....	286.57	106.1	−2.26	0.1034 ± 0.0223	1.327 ± 0.053
53173.455.....	296.33	96.0	−1.53	0.1006 ± 0.0219	1.289 ± 0.051
53173.478.....	302.55	88.5	−0.97	0.1254 ± 0.0259	1.214 ± 0.051
53175.400.....	279.81	112.5	−2.70	0.1858 ± 0.0503	1.205 ± 0.088
53175.443.....	294.41	98.2	−1.69	0.1640 ± 0.0405	1.180 ± 0.072
53175.484.....	305.19	84.7	−0.68	0.1068 ± 0.0251	1.239 ± 0.055
53176.406.....	282.88	109.6	−2.50	0.2647 ± 0.0802	1.077 ± 0.117
53176.446.....	296.27	96.1	−1.54	0.1610 ± 0.0481	1.177 ± 0.087
53176.498.....	308.17	79.6	−0.29	0.0782 ± 0.0228	1.290 ± 0.060
53177.470.....	303.18	87.6	−0.90	0.1270 ± 0.0546	1.209 ± 0.117
53182.449.....	289.23	35.9	−1.07	0.1772 ± 0.0771	1.179 ± 0.143
53182.485.....	297.53	26.8	−0.20	0.0790 ± 0.0329	1.334 ± 0.095
53183.331.....	240.18	64.4	−3.85	0.2535 ± 0.0648	1.286 ± 0.112
53183.375.....	263.39	53.4	−2.78	0.1380 ± 0.0346	1.369 ± 0.075
53184.364.....	259.29	55.5	−2.99	0.2736 ± 0.0565	1.162 ± 0.086
53184.401.....	275.39	46.4	−2.10	0.2227 ± 0.0466	1.166 ± 0.074
53184.438.....	287.68	37.3	−1.21	0.1897 ± 0.0396	1.166 ± 0.065
53185.393.....	273.55	47.5	−2.21	0.1718 ± 0.0548	1.256 ± 0.104
53185.425.....	284.49	39.9	−1.47	0.1960 ± 0.0629	1.169 ± 0.107
53185.453.....	292.24	33.0	−0.79	0.1874 ± 0.0590	1.151 ± 0.100
53185.485.....	298.95	24.8	−0.01	0.1621 ± 0.0512	1.165 ± 0.092

[a] P.A. is east of north.
[b] Errors have been normalized as discussed in § 4.

However, given the known rotational velocities of the calibration and check sources in this investigation, it is entirely reasonable to expect that examination of our check star as a UD as a function of baseline projection angle should result in a χ^2/dof of 1.0. For the sake of this investigation, we suggest that the true measurement uncertainty of the CHARA Array in the utilized operating mode is not fully characterized by merely tracking the measurement scatter as discussed in § 2 and that the actual error bars should be a factor of 3.42 larger than indicated by that scatter. In doing so, the χ^2/dof for HD 211833's UD fit becomes 1.0, and the indicated UD angular size is 1.235 ± 0.015 mas; as before, the ellipsoidal fit does not indicate a statistically significant improvement. We employ this scaling factor for the errors for examination of the Alderamin data in light of what should be the appropriate modeling context. The UD angular sizes as a function of baseline projection angle are seen in Figure 2.

From HD 211833's parallax of $\pi = 4.73 \pm 0.54$ (Perryman et al. 1997), we can derive a linear radius of $R = 28.1 \pm 3.2\ R_{\odot}$. The bolometric flux from § 3, in conjunction with the angular size, may be used to derive an effective temperature of $T_{\rm eff} = 4750 \pm 80$ K (see § 5.2 for details on this procedure). Both the radius and temperature numbers are consistent with our use of a K0-1II SED fitting template in § 3. The full characterization of HD 211833 that results from this ancillary investigation can be found in Table 6.

5. ALDERAMIN

5.1. *Apparent Stellar Disk*

The normalized values of V^2 for each observation of Alderamin are listed in Table 3, with their associated epoch, projected interferometer baseline length, position angle, and observation hour angle. A V^2 value is given for each observation, representing the individual visibility value derived from the two simultaneous measurements made on light output from either side of the beam recombination optic. Also given in Table 3 is an angular size for each individual V^2 from a UD fit (see eq. [1]), which for the purposes of this section alone will be used to provide an initial evaluation of the data. Some of the V^2 data points lie in the nonmonotonic region of a UD visibility curve (where $V^2 <\approx 0.02$ leads to multiple possible values of $\theta_{\rm UD}$); we assume for this first look at our data that the appropriate values

TABLE 5
RESULTS FROM SED FITS

STAR	SED TEMPLATE[a]	χ^2_ν	χ^2/dof	$F_{\rm bol}$ (10^{-8} ergs cm^{-2} s^{-1})	MODEL PARAMETERS	
					$\theta_{\rm SED}$ (mas)[b]	A_V
HD 197373	F5 IV	1.08	19.4/18	10.51 ± 0.17	0.412 ± 0.019	0.06 ± 0.018
HD 203280	A7 V	0.90	61.8/69	258.3 ± 1.42	1.36 ± 0.034	0 ± 0
HD 211833.....	K0–1 II	0.69	8.3/12	26.04 ± 1.67	1.32 ± 0.29	0.44 ± 0.042

[a] From Pickles (1998).
[b] Estimated angular size from SED fitting as described in § 3.

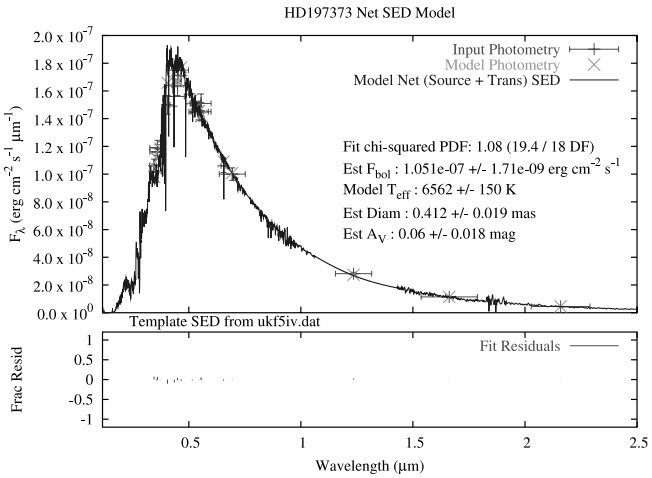

FIG. 1.—SED fitting for our calibrator star, HD 197373. In the top panel, the vertical bars on the data points are for the errors associated with those data points; the horizontal bars represent the bandpass of the data point. In the bottom panel, the fractional residuals (difference between data point & fit point, normalized by that data point) are given for each of those data points. [*See the electronic edition of the Journal for a color version of this figure.*]

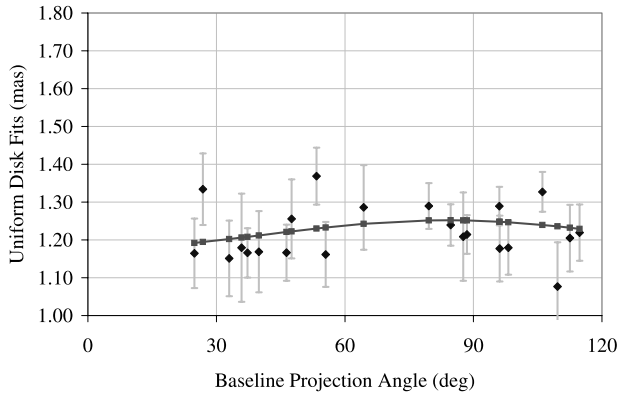

FIG. 2.—UD fits for the individual V^2 data points for HD 211833, as a function of baseline projection angle. The UD error bars in the figure are derived from V^2 errors using the scaling described in § 4. The square points are an ellipsoidal fit to the data, which for HD 211833 is indistinguishable from a straight line. [*See the electronic edition of the Journal for a color version of this figure.*]

of $\theta_{\rm UD}$ lie on the central lobe of a UD visibility function, noting that this assumption does not carry over into our physically more appropriate analysis of § 6. From those values, fitting a single global value of $\theta_{\rm UD}$ to the V^2 data ensemble results in a mean UD size of 1.607 ± 0.032 mas with $\chi^2/{\rm dof} = 4.484$. As is readily evident from Figure 3, a position-angle–independent fit would clearly be poor.

This discrepancy can be explored by relaxing the assumption of spherical symmetry and including the position angle of the observations in the fit. A spherical gaseous star will deform when rotating; such a shape projected onto the sky will appear, to first order, as an ellipse. For given physical situations, the true geometry of a rotating star will depart from that of an ellipsoid at the 5%–20% level; we return to this in a much more physically appropriate way in § 6. However, such a fit is useful as a mathematical construct to initially establish the position angle dependence of our angular size data. Using the basic equation for an ellipse,

$$\theta_{\rm UD}(\alpha) = \frac{2ab}{\sqrt{a^2 \sin^2(\alpha - \alpha_0) + b^2 \cos^2(\alpha - \alpha_0)}}, \quad (2)$$

we can solve for a projection-angle–dependent angular size, where $2a$ and $2b$ are the major and minor axes of the ellipse on the sky in mas, respectively, and α_0 is the orientation angle of the ellipse on the sky with $\alpha_0 = 0$ corresponding to the major axis pointing to the north on the sky and increasing to the east of north. Fitting equation (2) to the data in Table 2, we find that $2a = 1.625 \pm 0.056$ mas, $2b = 1.355 \pm 0.080$ mas, and $\alpha_0 = 3^\circ \pm 14^\circ$ with $\chi^2/{\rm dof} = 1.08$; this is a substantial improvement over the circular fit. An illustration of this fit and the UD data is seen in Figure 4 (see Table 7).

Other potential causes for Alderamin's departure from circularly symmetric V^2 data may be ruled out. If Alderamin were either a true or line-of-sight close binary star, our interpretation of the V^2 variations with baseline length and position angle would be incorrect. If a nearby binary were present in the interferometer beam, variations in the instrument's V^2 would be present in the data set, but as a function of time, and not just baseline projection angle.

We also consider two other potential deviations of the apparent disk of Alderamin from that of a uniform brightness distribution. The first, limb darkening, will affect a star's observed visibility curve and potentially bias our results. Second, for a rapidly rotating star, this phenomenon takes on an additional latitude dependence, often referred to in the literature as gravity darkening (e.g., Claret 2000). As first shown by von Zeipel (1924a), the polar zones of stars distorted by rapid rotation will be hotter than their equatorial zones, because the poles are closer to the center of the star. The consequential nonuniform flux distribution over the stellar surface affects a star's visibility curve. Our expectation is that the ellipsoidal fit in this section can be improved on by accounting for these effects, which we do in § 6.

TABLE 6
STELLAR PARAMETERS FOR THE CHECK STAR HD 211833 AS DERIVED FROM CHARA ANGULAR SIZE

Parameter	Value	Source
Apparent rotation velocity ($v \sin i$) (km s^{-1})	2	de Medeiros & Mayor (1999)
Spectral type	K3 III	Bidelman (1957); Schmitt (1971)
	K1 III	Wright et al. (2003)
	K0–1 II	§ 3
Parallax (π) (mas)	4.73 ± 0.54	Perryman et al. (1997)
Bolometric flux ($F_{\rm bol}$) (ergs cm^{-2} s^{-1})	26.04 ± 1.67	This work
Angular size (θ) (mas)	1.235 ± 0.015	This work
Effective temperature ($T_{\rm eff}$) (K)	4750 ± 80	This work
Linear radius (R) ($R_\odot$)	28.1 ± 3.2	This work

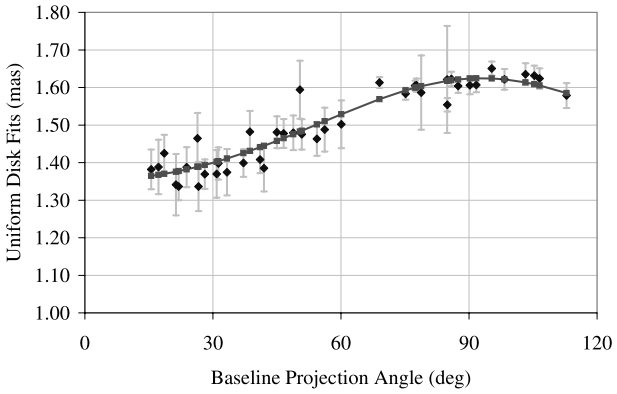

FIG. 3.—Same as Fig. 2, but for Alderamin. For Alderamin, the projection-angle–dependent ellipsoidal fit is significantly better than a single angular size fit to all of the visibility data, as described in § 5.1. [*See the electronic edition of the Journal for a color version of this figure.*]

5.2. *Effective Temperature*

Although we can compute a single effective temperature from our data on Alderamin, it must be stressed that this will be nothing more than a mathematical construct derived from geometrical considerations for the purposes of characterizing the gross properties of the star. Rewriting the stellar effective temperature equation in terms of the angular diameter and bolometric flux $F_{\rm bol}$, a value of $T_{\rm eff}$ was calculated from the flux and mean Rosseland diameter $\overline{\theta}_{\rm R}$, corresponding to the level in the atmosphere where the Rosseland mean opacity is unity, using

$$T_{\rm eff} = 2341\left(\frac{F_{\rm bol}}{\overline{\theta}_{\rm R}^2}\right)^{1/4} = 2341\left(\frac{F_{\rm bol}}{4a_{\rm R}b_{\rm R}}\right)^{1/4} \qquad (3)$$

where the units of $F_{\rm bol}$ are 10^{-8} ergs cm^{-2} s, and $\overline{\theta}_{\rm R}$, $a_{\rm R}$, and $b_{\rm R}$ are in mas. The error in $T_{\rm eff}$ is calculated from the usual propagation of errors applied to equation (3). The resultant mean $T_{\rm eff}$ for Alderamin is determined here from the flux value given in § 3 and the angular size data given in § 5.1 to be 7700 ± 170K. Previously, a value of 7773 K was estimated by Gray et al. (2003), which agrees well with our measure, noting again that this value for effective temperature is solely derived from geometric considerations and is an inadequate true characterization of a stellar surface over which the temperature, in fact, is latitude-dependent.

We should note, however, that this determination of $T_{\rm eff}$ differs from the values for pole and equator local effective temperatures that result from the Roche fitting in § 6. This is due to the accuracy with which the overall bolometric flux can be determined for Alderamin, using data across the spectrum from the *U* band (0.3 μm) to longward of the *M* band (5 μm). In contrast to that, the photometric fitting portion of the approach detailed in § 6 that constrains the pole temperatures of the models is limited by the accuracy with which the *V*- and *K*-band brightness of Alderamin has been determined, which is 2.44 ± 0.05 and 1.96 ± 0.05 (Johnson et al. 1966),[9] respectively.

A larger implication of this result is the potential inadequacy of effective temperatures derived from angular diameters at single projections across the disks of rotationally distorted stars. As we see in the next section, this effect can be much more significant than limb darkening in ascertaining a star's $T_{\rm eff}$, an effect which is expected to be routinely considered in all studies of stellar effective temperature.

[9] See footnote 8.

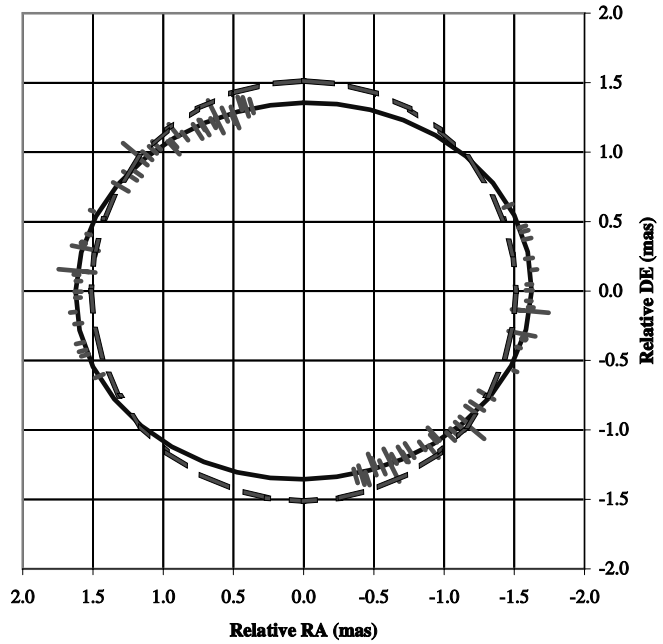

FIG. 4.—Data points along the limb of Alderamin for a simple ellipsoidal fit. The dashed line represents a circular fit for the same data. [*See the electronic edition of the Journal for a color version of this figure.*]

6. RAPID ROTATOR FITTING

The key to understanding the peculiar diameter results for Alderamin lies in its rapid rotation. The force of centrifugal acceleration at the equator, resulting from the rotation, offsets the effect of gravitation owing to the mass of the star. Under the conditions of hydrostatic equilibrium, uniform rotation, and a point mass gravitational potential, we can derive the equatorial rotational velocity, assuming we view the star at an inclination angle *i*. As developed in the work by Collins (1963, 1965) and presented in Jordahl (1972), the equation of shape for such a star under rotation may be written as

$$\frac{GM}{R_p(\omega)} = \frac{GM}{R(\theta,\ \omega)} + \frac{1}{2}\omega^2 R(\theta,\ \omega)^2 \sin^2\theta. \qquad (4)$$

From equation (4), we can arrive at an expression for the colatitude-dependent stellar radius at a rotation speed u:

$$r(\theta,\ u) = \frac{3}{u\sin\theta}\cos\left[\frac{\cos^{-1}(-u\sin\theta) + 4\pi}{3}\right], \qquad (5)$$

where u is the dimensionless rotation speed

$$\omega^2 = u^2\frac{8}{27}\frac{GM}{R_p^3(\omega)} \qquad (6)$$

and $r(\theta,\ u)$ is the radius normalized to the stellar polar radius for a given u. It is worth noting that, in contrast to our elliptical approximation in § 5.1, this approach solves for the expected shape of the stellar limb using an approach based on physics rather than merely geometry.

To interpret our interferometric data, we used a Monte Carlo approach that began by constructing models of Alderamin

TABLE 7
ALDERAMIN'S PARAMETERS DERIVED FROM THE DATA AND ASSEMBLED FROM THE LITERATURE

Parameter	Value	Reference
Values from the Literature		
Spectral type	A7 IV–V	Bidelman (1957)
Parallax (π) (mas)	66.84 ± 0.49	Perryman et al. (1997)
Bolometric flux ($F_{\rm bol}$) (10^{-8} ergs cm^{-2} s^{-1})	2583 ± 14	
Mass (M) (mas)	2.00 ± 0.15	This work
Metallicity ([Fe/H])	0.09	Gray et al. (2003)
Ellipsoidal Fit		
$2a_{\rm R}$ (mas)	1.625 ± 0.050	
$2b_R$ (mas)	1.355 ± 0.099	
Position angle (α) (deg)	3 ± 10	
R_a ($R_\odot$)	2.62 ± 0.08	
R_b ($R_\odot$)	2.18 ± 0.16	

based on rotation u and polar radius $R_p(\omega)$, sufficient to map the entire surface as a function of stellar colatitude and longitude. Model surfaces were constructed for the star at intervals of $0.^\circ8$ in both colatitude and longitude across the whole volume. Flux for a given surface area was then computed using the appropriate influence of gravity darkening (von Zeipel 1924a; Claret 2003), with $T_{\rm eff} \propto g^\beta$. For the models in question, pole temperature $T_{\rm pole}$ and gravity-darkening coefficient β were the free parameters that characterized this effect, following the relationship between local effective temperature, β, and local effective surface gravity:

$$T_{\rm local}(\theta) = T_{\rm pole}\left[\frac{g(\theta)}{g_{\rm pole}}\right]^\beta \quad (7)$$

as detailed in Collins (1965) and Domiciano de Souza et al. (2002). These models were then mapped onto the sky through the use of two additional free parameters describing orientation, inclination i, and on-sky rotational orientation α, with limb darkening appropriate for these model stars as indicated by Claret & Hauschildt (2003) applied at this point as well.

For comparison with interferometric data, the two-dimensional model star projected onto the sky was Fourier-transformed to provide model V^2 values for comparison with all observed visibility data points simultaneously. This transformation took into account a mild bandwidth smearing effect due to the data being taken through a broad K_s filter by repeating the calculation at a number of points through the filter and averaging the results. In addition, the temperature of each area element of a given model's sky projection would be used to compute a contribution to the overall apparent flux density from the star in both the V and K_s bands. The sum total of the apparent flux density was then compared to measured V and K_s band photometry for the star, thereby providing a constraint on $T_{\rm pole}$ for the models.

Thus, for a given set of six randomized free parameters $\{u,\ R_p(\omega),\ i,\ \alpha,\ \beta,\ T_{\rm pole}\}$, a 101,000 point volume surface was generated, projected on the sky, rotated, and the resultant image Fourier transformed for comparison to each of the observed V^2 data points, and a χ^2/dof calculated. The multidimensional downhill simplex method optimization code from Press et al. (1992) was then utilized to derive the best $\{u,\ R_p(\omega),\ i,\ \alpha,\ \beta,\ T_{\rm pole}\}$ solution from the random starting point, a process that typically took 500 iterations. In contrast to the earlier generation reduction code used in van Belle et al. (2001), this analysis compares the model and observed data in Fourier space, rather than image space, which will result in a more accurate result. In particular, some of the assumptions regarding UD geometry found in van Belle et al. (2001) are no longer invoked; the consideration of gravity darkening discussed above is possible only with this approach.

An exhaustive search of the rotating star parameter space was used to explore the χ^2/dof space through optimizations of over 1000 random starting points. Furthermore, a static grid of $\{u,\ i\}$ values was explored for optimal $\{R_p(\omega),\ \alpha,\ \beta,\ T_{\rm pole}\}$ values to ensure that no local minima were trapping the optimization code. The grid consisted of 1000 points spread uniformly over the space enclosed by $u = [0:1]$, $i = [0:90]$ and was run multiple times with random $\{R_p(\omega),\ \alpha,\ \beta,\ T_{\rm pole}\}$ seed values to ensure full mapping of the resultant $\{u,\ i\}$ χ^2/dof surface.

Once our best $\{u,\ R_p(\omega),\ i,\ \alpha,\ \beta,\ T_{\rm pole}\}$ solution and its associated χ^2/dof was established, errors for the individual parameters were derived. This was done by exploring the confidence region boundary through a modified version of our optimization code that searched the parameter space about our optimum six-parameter fit for appropriate increases in χ^2/dof. Each run of this modified code would target one of the six parameters for maximum deviation from its best-fit value, adjusting the six parameters toward that goal while maintaining the $\Delta\chi^2$/dof constraint. As with the original code, the modified code would start with randomized seed values of the six parameters, which in this case were slight deviations off of the best fit. Once done, the multidimensional downhill simplex method code would iterate to meet the $\Delta\chi^2$/dof condition and maximize the target parameter deviation. Through approximately a thousand runs of the code for each of the six parameters in question, the full confidence region boundary was explored and the appropriate error value was established for those parameters.

Trial runs of the χ^2/dof minimization technique using artificial data sets from synthetic stars were able to fully recover the initial four-parameter characterization for the original synthetic star. The model data sets covered a wide range of position angles, from 5° to 175° in 5° steps, and with visibility errors slightly better than in the Alderamin data set, which on average are 4% per measurement.

The best-fit model visibilities are seen in Figure 5, and the χ^2/dof surface resulting from the Alderamin data set is plotted in Figure 6, where $\{R_p(\omega),\ \alpha,\ \beta,\ T_{\rm pole}\}$ are optimized for

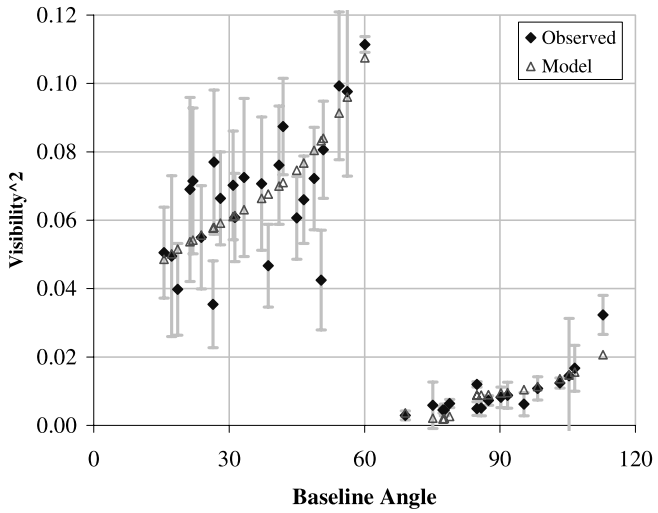

FIG. 5.—Squared visibility as a function of projected baseline angle for our observed data and the best-fit model. [*See the electronic edition of the Journal for a color version of this figure.*]

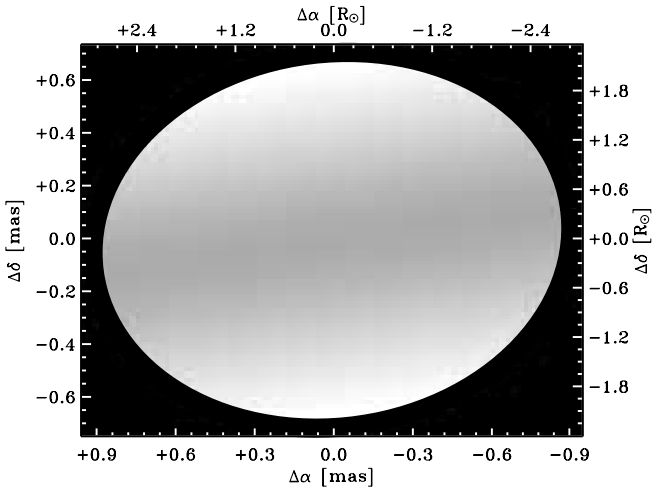

FIG. 7.—Best-fit three-dimensional model of Alderamin projected onto the sky. The polar regions have a temperature of $\sim 8440^{+430}_{-700}$ K, with equatorial regions being approximately 7600 K. [*See the electronic edition of the Journal for a color version of this figure.*]

minimum χ^2/dof for a given pair of $\{u, i\}$ coordinates. The six-parameter best-fit model's appearance on the sky is plotted in Figure 7. The best-fit value of $\chi^2/\mathrm{dof} = 2.16$ is slightly higher than the value for the ellipsoidal fit found in § 5.1, but this is due primarily to the additional complication of the fit found in incorporating the *V*- and K_s-band photometry constraints. From our solution values for these dimensionless parameters, we used values of $2.00 \pm 0.15\ M_\odot$ for the mass of Alderamin (derived in § 7) and a parallax of $\pi = 66.84 \pm 0.49$ mas (Perryman et al. 1997) to extract "real world" values such as rotation velocity and rotational period.

The difference between the primary and secondary axes of our best-fit model is $r_e(\omega) - r_p(\omega) = 201 \pm 32\ \mu$as, with an oblateness ratio of 1.298 ± 0.051. Our derived value for $v \sin i$ of 283 ± 19 km s^{-1} is in reasonable agreement with the larger spectroscopically determined values, as presented in § 1. Since our technique of mapping the surface (and in particular, the limb) of the star is sensitive to the highest velocity material of the star, we were not surprised that our $v \sin i$ is on the high end of the spectroscopically determined numbers; apparent velocities from spectra have to account for rotationally broadened spectral lines convolved across the entire surface of the star and could potentially underestimate values because of this approach. The dominant source of error in our technique is the mass estimate, which we discuss in the next section. The linear sizes are well constrained by the *Hipparcos* parallax, which has only a 0.4% quoted error.

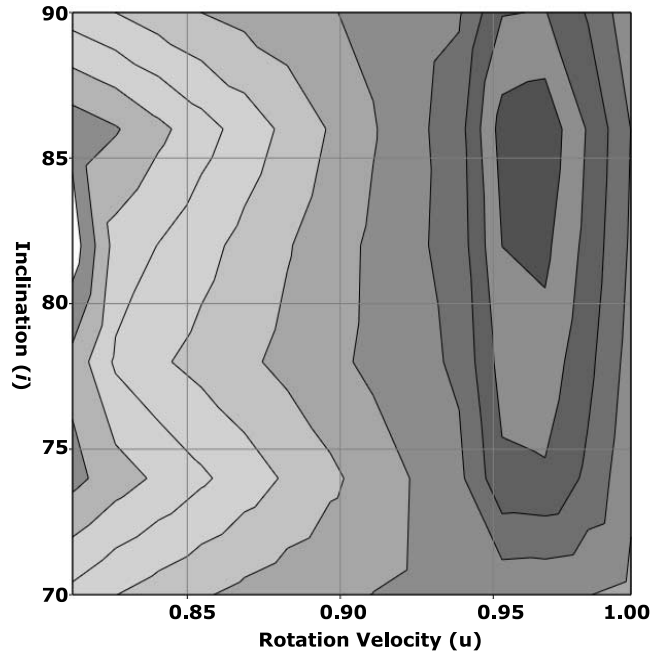

FIG. 6.—χ^2/dof surface for Alderamin as a function of rotation u and inclination i. Contour lines are in steps of $\Delta\chi^2/\mathrm{dof} = 0.5$ up from the minimum of $\chi^2/\mathrm{dof} = 2.16$ found at $\{u,\ i\} = \{0.9585,\ 88.2\}$. [*See the electronic edition of the Journal for a color version of this figure.*]

7. DISCUSSION

The breadth and depth of the parameters presented in Table 8 allow for a detailed examination of the present and past states of Alderamin. As discussed in Reiners (2003) and references therein, for spectral types later than A2, a gravity-darkening value of $\beta = 0.08$ is expected for these stars due to their outer convective envelopes. Our best-fit value of $\beta = 0.078^{+0.052}_{-0.059}$ is consistent with this expectation and lends a degree of confidence to the best-fit model. Although the errors on our model value are generous, they do indicate that a gravity-darkening value for a radiative envelope of $\beta = 0.25$ is not consistent with the best-fit model. (Running the data reduction code found in § 6 and restricting β to a value of 0.25, we find a global minimum with $\chi^2/\mathrm{dof} = 5.01$.)

The radii associated with Alderamin are somewhat larger than the typical values expected for a main-sequence A7 V star. Our previous investigation of the similarly rapidly rotating star Altair (van Belle et al. 2001), with an identical spectral type of A7 IV–V, indicates polar and equatorial sizes that are 30%–50% smaller. These increased sizes relative to Altair indicate to us that Alderamin is slightly evolved, perhaps being more adequately classified as an A7 IV; this finding is consistent with an age of 0.82 Gyr for Alderamin, as quoted by Rieke et al. (2005). This same study found only marginal evidence for excess flux at 24 μm, indicates that there is negligible excess at 2.2 μm, and is consistent with the 25 μm null result of Laureijs et al. (2002). These results are evidence that the observations presented here

TABLE 8

ALDERAMIN'S PARAMETERS DERIVED FROM THE GRAVITY- AND LIMB-DARKENED ROCHE MODELING

Parameter	Value
Primary Fitting Parameters	
Apparent polar radius $[r_p(\omega)]$ (mas)	$0.6753^{+0.0119}_{-0.0135}$
Position angle (α) (deg)	$17.2^{+3.2}_{-4.3}$
Gravity darkening (β)	$0.084^{+0.026}_{-0.049}$
Inclination (i) (deg)	$88.2^{+1.8}_{-13.3}$
Polar temperature ($T_{\rm pole}$) (K)	8440^{+430}_{-700}
Dimensionless velocity (u)	$0.9585^{+0.0197}_{-0.0116}$
χ^2/dof	2.16
Derived Values	
Apparent equatorial radius $[r_e(\omega)]$ (mas)	$0.8767^{+0.0293}_{-0.0183}$
Polar radius $[R_p(\omega)]$ ($R_\odot$)	2.175 ± 0.046
Equatorial radius $[R_e(\omega)]$ ($R_\odot$)	2.823 ± 0.097
Oblateness $[r_e(\omega)/r_p(\omega)]$	1.298 ± 0.051
Radii difference $[R_e(\omega) - R_p(\omega)]$ ($R_\odot$)	0.649 ± 0.107
Fractional breakup velocity (v_e/v_c)	$0.8287^{+0.0482}_{-0.0232}$
Equatorial velocity (v_e) (km s^{-1})	283 ± 19
Critical velocity (v_c) (km s^{-1})	342 ± 13
Apparent velocity ($v \sin i$) (km s^{-1})	283 ± 19
Period (P) (hr)	12.11 ± 0.26
Mass (M) ($M_\odot$)	2.00 ± 0.15

examine the photosphere of the star alone and are not contaminated by contributions from a circumstellar disk.

We can compare our data on Alderamin to the models of Girardi et al. (2000), which follow stars of a given mass through their evolution, predicting gravity and temperature; from the values of $\log g$ predicted for these models, we can derive linear radii. We can compare the location of Alderamin in radius-temperature space to these predicted tracks, as seen in Figure 8; solar metallicity tracks were used, given Alderamin's near-solar metallicity of $[{\rm Fe/H}] = 0.09$ (Gray et al. 2003), and the tracks all start an age of $\log T = 7.8$ and are stepped in increments of $\Delta \log T = 0.05$. From a simple examination of the location of Alderamin on this plot, three new aspects of the star appear to be revealed: First, its evolutionary status of tracking off of the main sequence is confirmed; second, the mass of the object appears to be $\sim 2.00 \pm 0.15\ M_\odot$, which is consistent with Malagnini & Morossi (1990); third, its age appears to be $\log T \sim 8.9$, roughly 800 Myr, which is consistent with the finding of Rieke et al. (2005). However, basing these interpretations on these models in particular may be suspect, since the impact of Alderamin's extreme rotation probably alters its specific isochrone. We can illustrate this by considering the rotation history of the object through conservation of angular momentum.

The moment of inertia for a star may be written as

$$I = k^2 M R^2, \tag{8}$$

where k^2 is the radius of gyration (Stepień 2000); $k^2 = 0.20$ for the fully convective case, whereas $k^2 = 0.05$ for the fully radiative case. Although Alderamin's value for k^2 is not known in detail, we can consider it for the moment to be constant over the star's recent evolution off of the main sequence. From the Girardi et al. (2000) plots in Figure 8, we can estimate the average linear size of Alderamin to have increased from ~ 1.6 to $1.8\ R_\odot$ to its current value of $\sim 2.54\ R_\odot$. However, by conservation of angular momentum, the star's rotation speed when it was this smaller size would have been $v_e/v_c \simeq 0.92-0.98$, very nearly rotational breakup speed. Such a previous speed is not impossible from dynamical considerations alone but is far greater than 90% of breakup, which has been argued to be the expected upper limit due to star formation considerations, although this limit is not borne out by the observations (Stassun et al. 1999; Rebull 2001).

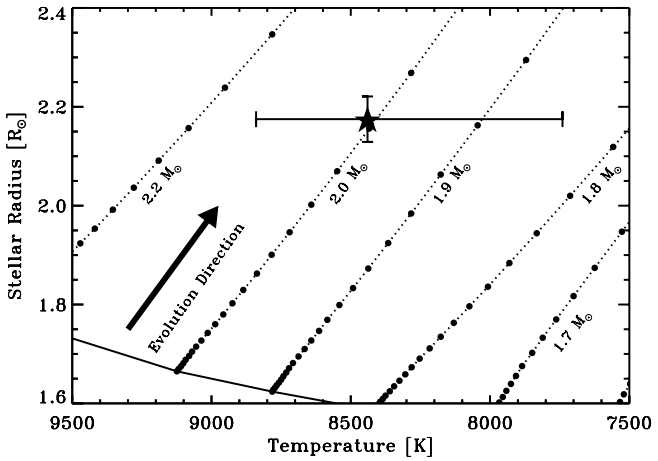

FIG. 8.—Alderamin as located on the radius-temperature evolutionary tracks of Girardi et al. (2000). Solar metallicity tracks were used, consistent with Alderamin's metallicity of $[{\rm Fe/H}] = 0.09$ (Gray et al. 2003), and the tracks all start an age of $\log T = 7.8$, being stepped in increments of $\Delta \log T = 0.05$.

As such, one of two circumstances may have affected the rotation history of Alderamin, independently or in unison. First, the moment of inertia may have changed through differences in the radius of gyration as the ratio of convective to radiative portions of the star changed. Second, the Girardi et al. (2000) evolutionary tracks potentially do not properly describe the radius history of a rapid rotator such as Alderamin. Considerable work on the impact of rapid rotation on the evolution of massive stars ($M \geq 9\ M_\odot$) has been done by Maeder & Meynet (see, e.g., Maeder & Meynet 2000), but $\simeq 2\ M_\odot$ solar metallicity model tracks do not appear readily available. Alternatively, rotation speeds in excess of 90% of $v_{\rm crit}$ may be allowed in extreme cases such as these.

8. CONCLUSIONS

We have measured the visibility varying due to the apparent oblateness of Alderamin's disk on the sky and modeled those data with an appropriate Roche model. This approach allows for an interferometric measurement of the true stellar rotation velocity and latitude-dependent temperature structure, which in turn enabled a more detailed investigation into the underlying rotation environment of this star, and its angular momentum history, than could be afforded by previous spectroscopic measurements of $v \sin i$. The determination of the star's gravity darkening from spatial data alone is a unique challenge to stellar models and consistent with those theoretical expectations. Such rotational speed and shape determinations can also potentially be useful for evaluating stellar seismology data (Gizon & Solanki 2004). Furthermore, we have demonstrated a technique that can recover a level of detail on rapidly rotating stars that heretofore had been out of reach of direct observational techniques. Verifying a larger test interferometric cohort around less rapidly spinning stars undoubtedly could be key to advances in stellar science.

As detailed in van Belle et al. (2004), a simple examination of the rotational velocity catalog collated by Bernacca & Perinotto (1973) indicates there are over 70 known bright ($V < 4$) main-sequence stars in the northern hemisphere that are rapid rotators

with $v \sin i > 200$ km s^{-1}; examination of bright ($V < 8$) evolved objects in de Medeiros & Mayor (1999) that have $v \sin i > 15$ km s^{-1} indicates there are over 70 potential targets as well. Objects that fit these criteria should exhibit apparent flattening of their disks at the $\approx$10% level. Clearly, there are numerous opportunities to implement this technique with the new generation of long-baseline optical and infrared interferometers such as the CHARA Array, NPOI, and VLTI, which all have multiple baselines allowing the required stellar disk projection measurements to be made in much shorter observing times. Our CHARA Array follow-up observing campaign of other rapidly rotating stars already has initial results that support this promising line of research.

We would like to thank Mel Dyck for first suggesting to us the possibility of utilizing oblateness measurements to derive rotational velocity, Doug Gies for a large array of useful comments on our manuscript, and Antoine Mérand for particularly useful suggestions regarding bandwidth smearing as it pertained to the analysis in § 6. Portions of this work were performed at the California Institute of Technology under contract with the National Aeronautics and Space Administration. This research has been supported by National Science Foundation grants AST 02-05297 and AST 03-07562. Additional support has been received from the Research Program Enhancement program administered by the Vice President for Research at Georgia State University.

APPENDIX

A PRIORI OBLATENESS ESTIMATE FOR RAPID ROTATORS

Outside of the rigorous mathematical analysis of observed V^2 data for rapid rotators, it is useful to have a shorthand approximation of what the expected oblateness for a rapid rotator should be. This is particularly useful for developing target lists of these types of objects for the CHARA Array and other interferometers. The force of centripetal acceleration at the equator, resulting from the rotation, offsets the effect of gravitation owing to the mass of the star. Under the conditions of hydrostatic equilibrium, uniform rotation, and a point mass gravitational potential, we can derive the equatorial rotational velocity, assuming we view the star at an inclination angle i. Under these conditions, we have that

$$v \sin i \approx \sqrt{\frac{2GM}{R_b}\left(1 - \frac{R_b}{R_a}\right)}, \tag{A1}$$

where R_b and R_a are the apparent minor and major stellar radii, and M is the stellar mass (cf. Brouwer & Clemence 1961; Elliot & Nicholson 1984; Baron et al. 1989). Using catalog measurements of $v \sin i$ (e.g., Glebocki & Stawikowski 2000) and a reasonable estimate for M and $\overline{R}$ (for use as R_b) derived from spectral type, an estimate of the size ratio R_b/R_a may be established.

As an example, Malagnini & Morossi (1990) estimate the mass of Alderamin at $1.90 \pm 0.29\ M_\odot$; an A7 IV–V star should have an approximate radius of $\overline{R} = 2.1\ R_\odot$ (Cox 2000); in conjunction with a spectroscopic $v \sin i$ estimate of $\sim$245 km s^{-1} (Bernacca & Perinotto 1970), we find that R_b/R_a should be approximately $\sim$1.21, which is in good agreement with the solutions presented in Table 8.

REFERENCES

Abt, H. A., & Morrell, N. I. 1995, ApJS, 99, 135
Abt, H. A., & Moyd, K. I. 1973, ApJ, 182, 809
Baron, R. L., French, R. G., & Elliot, J. L. 1989, Icarus, 78, 119
Bernacca, P. L., & Perinotto, M. 1970, Contrib. Oss. Astrofis. Univ. Padua, 239, 1
———. 1973, A Catalog of Stellar Rotational Velocities (Padua: Unit. Padua)
Bidelman, W. P. 1957, PASP, 69, 326
Blackwell, D. E., & Lynas-Gray, A. E. 1998, A&AS, 129, 505
Boden, A. F., et al. 1998, ApJ, 504, L39
Brouwer, D., & Clemence, G. M. 1961, in The Solar System III, ed. G. P. Kuiper & B. M. Middlehurst (Chicago: Univ. Chicago Press), 31
Claret, A. 2000, A&A, 359, 289
———. 2003, A&A, 406, 623
Claret, A., & Hauschildt, P. H. 2003, A&A, 412, 241
Collins, G. W., II. 1963, ApJ, 138, 1134
———. 1965, ApJ, 142, 265
Collins, G. W., II, & Harrington, J. P. 1966, ApJ, 146, 152
Collins, G. W., II, & Smith, R. C. 1985, MNRAS, 213, 519
Cox, A. N. 2000, Allen's Astrophysical Quantities, ed. A. N. Cox (4th ed.; New York: AIP)
Crawford, D. L., Barnes, J. V., Faure, B. Q., & Golson, J. C. 1966, AJ, 71, 709
Davis, J., Tango, W. J., & Booth, A. J. 2000, MNRAS, 318, 387
de Medeiros, J. R., Mayor, M. 1999, A&AS, 139, 433
Domiciano de Souza, A., Kervella, P., Jankov, S., Abe, L., Vakili, F., di Folco, E., & Paresce, F. 2003, A&A, 407, L47
Domiciano de Souza, A., Vakili, F., Jankov, S., Janot-Pacheco, E., & Abe, L. 2002, A&A, 393, 345
Douglas, A. V. 1926, ApJ, 64, 262
Dyck, H. M., Benson, J. A., van Belle, G. T., & Ridgway, S. T. 1996, AJ, 111, 1705
Eggen, O. J. 1963, AJ, 68, 697
———. 1972, ApJ, 175, 787
Elliot, J. L., & Nicholson, P. D. 1984, in Planetary Rings, ed. R. Greenberg & A. Brahic (Tucson: Univ. Arizona Press), 25
Girardi, L., Bressan, A., Bertelli, G., & Chiosi, C. 2000, A&AS, 141, 371
Gizon, L., & Solanki, S. K. 2004, Sol. Phys., 220, 169
Glebocki, R., & Stawikowski, A. 2000, Acta Astron., 50, 509
Gray, D. F. 1980, PASP, 92, 771
Gray, R. O., Corbally, C. J., Garrison, R. F., McFadden, M. T., & Robinson, P. E. 2003, AJ, 126, 2048
Henry, G. W., Fekel, F. C., Henry, S. M., & Hall, D. S. 2000, ApJS, 130, 201
Johnson, H. L. 1968, in Stars and Stellar Systems 7, Nebulae and Interstellar Matter, ed. B. M. Middlehurst & L. H. Aller (Chicago: Univ. Chicago Press), chap. 5
Johnson, H. L., Iriarte, B., Mitchell, R. I., & Wisniewskj, W. Z. 1966, Commun. Lunar Planet. Lab., 4, 99
Johnson, H. L., & Morgan, W. W. 1953, ApJ, 117, 313
Jordahl, P. R. 1972, Ph.D. thesis, Univ. Texas at Austin
Kornilov, V. G., et al. 1991, Trudy Gosud. Astron. Inst., 63, 4
Laureijs, R. J., Jourdain de Muizon, M., Leech, K., Siebenmorgen, R., Dominik, C., Habing, H. J., Trams, N., & Kessler, M. F. 2002, A&A, 387, 285
Maeder, A. 1997, A&A, 321, 134
———. 2000, NewA Rev., 44, 291
Maeder, A., & Meynet, G. 2000, ARA&A, 38, 143
Mathis, J. S. 1990, ARA&A, 28, 37
Malagnini, M. L., & Morossi, C. 1990, A&AS, 85, 1015
Martin, E. L., & Claret, A. 1996, A&A, 306, 408
McAlister, H. A., et al. 2005, ApJ, 628, 439
Moreno, H. 1971, A&A, 12, 442
Mozurkewich, D., et al. 1991, AJ, 101, 2207
Ohishi, N., Nordgren, T. E., & Hutter, D. J. 2004, ApJ, 612, 463
Perryman, M. A. C., et al. 1997, A&A, 323, 49

Peterson, D. M., et al. 2006, ApJ, in press
Pickles, A. J. 1998, PASP, 110, 863
Piirola, V. 1976, Obs. Astrophys. Lab. Univ. Helsinki Rep., 1
Press, W. H., Teukolsky, S. A., Vetterling, W. T., & Flannery, B. P. 1992, Numerical Receipes in C: The Art of Scientific Computing (Cambridge: Cambridge Univ. Press)
Quirrenbach, A., Buscher, D. F., Mozurkewich, D., Hummel, C. A., & Armstrong, J. T. 1994, A&A, 283, L13
Rebull, L. M. 2001, AJ, 121, 1676
Reiners, A. 2003, A&A, 408, 707
Rieke, G. H., et al. 2005, ApJ, 620, 1010
Schlesinger, F. 1909, Publ. Allegheny Obs., 1, 134
———. 1911, MNRAS, 71, 719
Schmitt, J. L. 1971, ApJ, 163, 75
Slettebak, A. 1949, ApJ, 110, 498
———. 1955, ApJ, 121, 653
———. 1966, ApJ, 145, 126
Stassun, K. G., Mathieu, R. D., Mazeh, T., & Vrba, F. J. 1999, AJ, 117, 2941
Stepień, K. 2000, A&A, 353, 227
ten Brummelaar, T., et al. 2005, ApJ, 628, 453
Uesugi, A., & Fukuda, I. 1982, Revised Catalog of Stellar Rotational Velocities (Kyoto: Univ. Kyoto)
van Belle, G. T., Ciardi, D. R., Thompson, R. R., & Akeson, R. L. 2004, in IAU Symp. 215, Stellar Rotation, ed. A. Maeder & P. Eenens (San Francisco: ASP), 177
van Belle, G. T., Ciardi, D. R., Thompson, R. R., Akeson, R. L., & Lada, E. A. 2001, ApJ, 559, 1155
van Belle, G. T., & van Belle, G. 2005, PASP, 117, 1263
von Zeipel, H. 1924a, MNRAS, 84, 665
———. 1924b, MNRAS, 84, 684
Wright, C. O., Egan, M. P., Kraemer, K. E., & Price, S. D. 2003, AJ, 125, 359
Zahn, J.-P. 1992, A&A, 265, 115
Zdanavicius, K., et al. 1969, Vilnius Astron. Obs. Biuletenis, 26, 3
———. 1972, Vilnius Astron. Obs. Biuletenis, 34, 3